Research Article **Open Access**

Alfredo N. Wetzel*, Leslie M. Smith, and Samuel N. Stechmann

Moisture Transport due to Baroclinic Waves: Linear Analysis of Precipitating Quasi-Geostrophic Dynamics

https://doi.org/10.1515/mcwf-2017-0002
Received February 23, 2017; accepted July 26, 2017

Abstract: The effects of rainfall speed, V_T, and meridional/vertical moisture gradients on the meridional moisture transport are examined in the context of mid-latitude baroclinic waves. These effects are investigated in an idealized model that can be solved analytically. The model is systematically derived in a precipitating quasi-geostrophic limit, starting from a moist atmospheric model with minimal representation of cloud microphysics. Single-phase dynamics are considered, with a comparison of three cases: unsaturated, saturated with $V_T = 0$, and saturated with $V_T > 0$. The Eady problem for linear baroclinic waves is analyzed, with modifications to incorporate moisture. As a preliminary step, the moist waves are shown to have properties consistent with prior studies, including larger growth rates and smaller spatial scales in the saturated cases in comparison to the classic dry Eady problem. Then, in addition, it is shown that the meridional moisture flux, as a function of height, has a mid-tropospheric maximum in the case of $V_T = 0$, and a maximum in the lower troposphere or at the surface for sufficiently large values of V_T. These results for different V_T values are discussed in the context of meridional moisture transport in observational data.

Keywords: meridional moisture transport, moist baroclinic waves, moist baroclinic instability, precipitating quasi-geostrophic dynamics.

MSC: 35B30, 35Q35, 76E20, 76U05, 86A10

1 Introduction

Atmospheric transport of heat and moisture from the equator to the poles is of principal importance for the Earth's meteorology and climatology [16, 23, 28]. Transient (baroclinic) waves or eddies are a primary mechanism for this mid-latitude meridional transport; for example, see Peixoto and Oort [25, Fig. 12.11b] and Trenberth and Stepaniak [29, Fig. 1]. In this manner, mid-latitude heat and water transport by baroclinic waves accounts for a substantial portion of the Earth's energy budget and is of critical importance to understanding sensible and latent heating in the atmosphere.

A simple theoretical framework for the transport of heat in the mid-latitude atmosphere, in the context of baroclinic waves and their stability, is provided by the pioneering work of Charney [4] and Eady [7]. Primarily, their work focused on large/synoptic-scale phenomena with a simple baroclinic background profile. This naturally gave rise to the, now well-established, quasi-geostrophic (QG) equations and has led to the understanding of baroclinic wave instability as, essentially, a synoptic-scale event. Though their emphasis was

***Corresponding Author: Alfredo N. Wetzel:** Department of Mathematics, University of Wisconsin–Madison, Madison, Wisconsin, USA, Email: alfredo.wetzel@wisc.edu
Leslie M. Smith: Department of Mathematics & Department of Engineering Physics, University of Wisconsin–Madison, Madison, Wisconsin, USA, Email: lsmith@math.wisc.edu
Samuel N. Stechmann: Department of Mathematics & Department of Atmospheric and Oceanic Sciences, University of Wisconsin–Madison, Madison, Wisconsin, USA, Email: stechmann@wisc.edu

not directly on (sensible) heat transport, heat transport can be readily computed from their analyses [e.g., 24] but not moisture transport or the effects of moisture.

Inclusion of water and the effects of moisture into theoretical studies of baroclinic waves has drawn much attention and a variety of approaches. The interaction between condensational heating effects and baroclinic instability make this, however, a difficult analytical problem due to non-linearities arising from phase changes and non-trivial equation coupling. Principal avenues of study of moist condensation and latent heat release in baroclinic waves/instability include models of shallow-water [17], quasi-geostrophic [2, 5, 18, 19, 21, 31], semi-geostrophic [8], and primitive [9, 11, 12] equation dynamics. A number of these studies include moisture effects implicitly, in the form of ascending/moist and descending/dry air [8, 9] or the wave-CISK (conditional instability of the second kind) parametrization [2, 5, 19, 31], while not directly incorporating moisture dynamics. Overwhelmingly it is found that latent heat release increases the growth rate of the instability; in some cases it additionally decreases the most unstable wavenumber. Essentially this outcome can be understood as the latent heat reducing the "effective" stability of the flow. For this reason, it is sometimes useful to avoid the dynamical perspective altogether and proceed to account for the effects of moisture using effective values of the static stability and attempt to quantify this quantity either analytically or empirically [6, 10, 22, 26].

In the present paper, we study the effects of meridional/vertical background moisture gradients and rainfall speed V_T on the meridional water transport. In particular, we use the Eady problem framework and accompanying normal mode solutions to derive straightforward formulas for the meridional moisture transport and determine its dependence on key moisture parameters.

To study the effects of moisture on meridional transport, we use the fast autoconversion and rain evaporation (FARE) model of Hernández-Dueñas et al. [13] in the precipitating quasi-geostrophic (PQG) limit [27]. The FARE model consists of a "minimal" thermodynamics and microphysics description of the atmosphere and therefore acts as an amenable starting point for this study. Moreover, the FARE model allows water to precipitate out of the domain (sedimentation) in the form of rainfall, with a chosen rainfall speed V_T. Rainfall speed thus becomes a tunable parameter which has significant effects on the qualitative and quantitative structure of the rainwater content. We simplify our study even further by considering linear perturbations about a single-phase background state (unsaturated or saturated only, since perturbations are small) and attribute differences that arise between the solutions to the phase change. The relative simplicity of this setup then allows us to obtain analytically tractable formulas and determine the relative parameter dependence of the moisture transport on the moisture parameters.

The paper is organized as follows: in Section 2, we describe the relevant preliminary information about the FARE Model. First, we present the FARE model equations and discuss how phase changes are handled. Second, we discuss the decomposition of thermodynamic variables between background and anomalies in unsaturated and saturated regimes and present the PQG equations. In Section 3, we study the linear instability of the PQG model. In particular, we derive – using standard methods – the normal mode solutions of the Eady problem and discuss their similarity with the "dry" Eady solutions. We then briefly discuss the growth rate of the instability, our chosen normalization of the normal modes, and suitable results concerning the meridional heat flux. In Section 4, we present our primary result on the meridional water transport. We discuss the effects of background moisture and rainfall speed in three distinct cases: unsaturated regime, saturated regime with $V_T = 0$, and saturated regime with $V_T > 0$. Finally, these results for different V_T values are discussed in the context of meridional moisture transport in observational data.

2 Description of the Precipitating Quasi-Geostrophic Equations

In this section, the precipitating quasi-geostrophic (PQG) equations are described. In order to allow a linear analysis, single-phase dynamics are considered separately for the unsaturated and saturated phases.

Table 1: List of thermodynamic variables used in this paper. All variables listed, except $\tilde{q}_{vs}$, are anomalies from the anelastic background state.

Variable	Definition
q_r	Rainwater mixing ratio
q_v	Water vapor mixing ratio
$\tilde{q}_{vs}$	Saturation water vapor mixing ratio
$q_t = q_v + q_r$	Total water mixing ratio
θ	Potential temperature
$\theta_e = \theta + (L_v/c_p)q_v$	Equivalent potential temperature (linearized)

2.1 Starting Point: A Cloud-Resolving Model with Minimal Microphysics

To study the effects of moisture on mid-latitude dynamics, we use a quasi-geostrophic model that can be derived from a cloud-resolving model with minimal microphysics. This minimal cloud-resolving model is the Fast Autoconversion and Rain Evaporation (FARE) model of Hernández-Dueñas et al. [13]. The FARE model is minimal in the sense that fast time scales are assumed in the phase changes of water constituents. These fast microphysics completely eliminate the cloud water constituent of moisture and retain only water vapor q_v and rainwater q_r. The FARE model presents tractable analytical properties that preserve key microphysics, as discussed in Hernández-Dueñas et al. [13] and Hernández-Dueñas et al. [14].

The FARE model with the addition of Coriolis force is given by the system of equations [13, eqns. 2.35–2.38]

$$\frac{D\boldsymbol{u}}{Dt} + f\mathbf{k}\times\boldsymbol{u} = -\boldsymbol{\nabla}\left(\frac{p}{\rho_0}\right) + \mathbf{k}b(\theta^{\text{tot}}, q_v^{\text{tot}}, q_r^{\text{tot}}, z), \tag{1a}$$

$$\boldsymbol{\nabla}\cdot\boldsymbol{u} = 0, \tag{1b}$$

$$\frac{D\theta_e^{\text{tot}}}{Dt} = 0, \tag{1c}$$

$$\frac{Dq_t^{\text{tot}}}{Dt} - V_T\frac{\partial q_r^{\text{tot}}}{\partial z} = 0, \tag{1d}$$

where $\boldsymbol{u} = (u, v, w)$ corresponds to the three-dimensional velocity, p is the pressure, θ is the potential temperature, θ_e is the linearized equivalent potential temperature (cf. (6)), buoyancy b is given by

$$b = b(\theta^{\text{tot}}, q_v^{\text{tot}}, q_r^{\text{tot}}, z) = g\left(\frac{\theta^{\text{tot}} - \tilde{\theta}}{\theta_0} + \varepsilon_0\left(q_v^{\text{tot}} - \tilde{q}_v\right) - \left(q_r^{\text{tot}} - \tilde{q}_r\right)\right), \tag{2}$$

and q_v, q_r, q_t correspond to the mixing ratios of water vapor, rainwater, and total water, respectively. Here, $\mathbf{k}$ corresponds to the vertical unit vector and the material derivative D/Dt is defined as $D/Dt = \partial/\partial t + \boldsymbol{u}\cdot\boldsymbol{\nabla}$. In addition, ρ_0 is a reference density, f is the Coriolis parameter, and V_T is the constant rainfall speed. All thermodynamic variables are assumed to be unknown functions of the position $\mathbf{x}$ and time t. We use the superscript "tot" (i.e., total) to denote that the given thermodynamic variable includes both a background anelastic state, denoted with $\tilde{(\cdot)}$, and an anomaly. A comprehensive list of relevant thermodynamics variables and parameters used throughout the paper is given in Table 1 and Table 2, respectively.

By definition, all thermodynamic variables are decomposed into background and anomaly components, e.g., $q_t^{\text{tot}}(\mathbf{x}, t) = \tilde{q}_t(z) + q_t(\mathbf{x}, t)$, where the background states are assumed to be linear functions of height z only. In terms of these background states, the FARE equations (1a)–(1d) then become

$$\frac{D\boldsymbol{u}}{Dt} + f\mathbf{k}\times\boldsymbol{u} = -\boldsymbol{\nabla}\left(\frac{p}{\rho_0}\right) + \mathbf{k}b(\theta, q_v, q_r), \tag{3a}$$

Table 2: List of parameters used in this paper with typical (northern hemisphere) mid-latitude values.

Parameter	Typical Value	Definition
ρ_0		Reference density
θ_0	300 K	Reference potential temperature
Θ	3 K	Background potential temperature gradient
f	10^{-4} s^{-1}	Coriolis parameter
V_T	0.3 – 10 m s^{-1}	Velocity of rain precipitation
L_v	2.5×10^6 J kg^{-1}	Latent heat factor
c_p	10^3 J kg^{-1} K^{-1}	Specific heat at constant pressure
$\varepsilon_0 = R_v/R_d - 1$	0.6	R_v is water vapor gas constant, R_d is dry air gas constant
L	1, 000 km	Horizontal reference scale for QG dynamics
H	10 km	Vertical reference scale for QG dynamics
$d\tilde{\theta}/dz$	3 K km^{-1}	Background temperature gradient
L_d	990 km	Dry deformation radius
$d\tilde{q}_v/dz$	−1.3 g kg^{-1} km^{-1}	Background water vapor gradient
$\overline{Q}_v^{dim}$	0.17 g kg^{-1} degree^{-1}	Meridional water vapor gradient
$\overline{Q}_v$	1.25	Meridional water vapor gradient (non-dimensional)
G_u	1.08	Unsaturated vertical moisture gradient ratio
$d\tilde{q}_{vs}/dz$	−0.8 g kg^{-1} km^{-1}	Saturation water vapor gradient
L_{de}	572 km	Moist deformation radius
$\overline{Q}_r^{dim}$	0.13 g kg^{-1} degree^{-1}	Meridional rainwater gradient
$\overline{Q}_r$	1	Meridional rainwater gradient (non-dimensional)
G_s	0.67	Saturated vertical moisture gradient ratio

$$\nabla \cdot \boldsymbol{u} = 0, \tag{3b}$$

$$\frac{D\theta_e}{Dt} + w\frac{d\tilde{\theta}_e}{dz} = 0, \tag{3c}$$

$$\frac{Dq_t}{Dt} + w\frac{d\tilde{q}_t}{dz} = V_T\frac{d\tilde{q}_r}{dz} + V_T\frac{\partial q_r}{\partial z}. \tag{3d}$$

Phase changes in the water content are accounted for in the FARE model by determining whether the water vapor q_v^{tot} at a given location is less than or equal to the saturation water vapor $\tilde{q}_{vs}$. Any 'excess' q_v^{tot} above the saturation water vapor immediately condenses into rainwater q_r^{tot}; phase changes are assumed to occur immediately. Namely,

$$q_v^{\text{tot}}(\mathbf{x}, t) < \tilde{q}_{vs}(z) \quad \text{and} \quad q_r^{\text{tot}}(\mathbf{x}, t) = 0 \quad \text{(unsaturated)}, \tag{4a}$$

$$q_v^{\text{tot}}(\mathbf{x}, t) = \tilde{q}_{vs}(z) \quad \text{and} \quad q_r^{\text{tot}}(\mathbf{x}, t) \geq 0 \quad \text{(saturated)}. \tag{4b}$$

To simplify the analysis, we limit ourselves to purely saturated and unsaturated dynamics; a prescribed unsaturated or saturated basic state whose perturbations remain unsaturated or saturated. Therefore, the background states $\tilde{(\cdot)}$ in each phase studied are different. Due to the restrictions imposed by phase changes (4a)–(4b) on relevant background states, the definition of the buoyancy (2) changes in unsaturated and saturated regimes.

Table 3: Appropriate variable scalings (reference scales) for non-dimensionalization.

Variable	Scale
x, y	L
z	H
t	L/U
u, v	U
w	$W = UH/L$
p	P
θ, θ_e	Θ
q_v, q_r, q_t	$Q = c_p\Theta/L_v$
b, b_u, b_s	$B = g\Theta/\theta_0$

2.2 QG Equations in the Unsaturated Regime

The PQG equations are obtained from suitable asymptotic analysis of the FARE equations of Hernández-Dueñas et al. [13]. In essence, the derivation of PQG amounts to the systematic selection of significant (leading order and first-order correction) terms of the evolution equations when rotation and stratification are strong. The derivation is similar to the derivation of the dry QG equations, with modifications to account for moisture; for example, an assumption of strong stratification is utilized, where the stratification is measured by the potential temperature or equivalent potential temperature depending on the phase (unsaturated or saturated, respectively). In the QG limit, the evolution equations consist of the 'dry' dynamics with an additional moisture equation. The interested reader is referred to Smith and Stechmann [27] for additional details concerning the PQG derivation.

In this section, we specify the decomposition of the thermodynamic variables into a background anelastic state and anomaly when the dynamics are unsaturated; equation (4a). We suppose that our background state consists of known unsaturated functions $\tilde{q}_v$, $\tilde{q}_r$ and deviations from these background states never become saturated; namely, $\tilde{q}_v < \tilde{q}_{vs}$, $\tilde{q}_r = 0$, and $q_r = 0$.

In the unsaturated regime, the buoyancy (2) then becomes

$$b = b_u(\theta, q_v) = g\left(\frac{\theta}{\theta_0} + \varepsilon_0 q_v\right). \tag{5}$$

So, in the unsaturated state, the relevant thermodynamic variables are the water vapor q_v and the potential temperature θ. Moreover, we use a separation that preserves a similar relation between the anomalies and the "total" variables:

$$\begin{bmatrix}\tilde{\theta}_e \\ \tilde{q}_t\end{bmatrix} = \begin{bmatrix}1 & \frac{L_v}{c_p} \\ 0 & 1\end{bmatrix}\begin{bmatrix}\tilde{\theta} \\ \tilde{q}_v\end{bmatrix} \quad \text{and} \quad \begin{bmatrix}\theta_e \\ q_t\end{bmatrix} = \begin{bmatrix}1 & \frac{L_v}{c_p} \\ 0 & 1\end{bmatrix}\begin{bmatrix}\theta \\ q_v\end{bmatrix}. \tag{6}$$

The thermodynamic equations (3c)–(3d) of the FARE model then become

$$\frac{D\theta}{Dt} + w\frac{d\tilde{\theta}}{dz} = 0 \quad \text{and} \quad \frac{Dq_v}{Dt} + w\frac{d\tilde{q}_v}{dz} = 0. \tag{7}$$

The equations in (7) may also be combined to form an equation for the buoyancy (5). Namely,

$$\frac{Db_u}{Dt} + wN_u^2 = 0, \quad \text{where} \quad N_u^2 = g\left(\frac{1}{\theta_0}\frac{d\tilde{\theta}}{dz} + \varepsilon_0\frac{d\tilde{q}_v}{dz}\right). \tag{8}$$

In the QG limit, under the non-dimensionalization shown in Table 3, the non-dimensional first-order correction evolution equations are [27]

$$\frac{D_H\zeta}{Dt} = \frac{\partial w}{\partial z}, \tag{9a}$$

$$\frac{D_H b_u}{Dt} + \frac{L_d}{L} w = 0, \tag{9b}$$

$$\frac{D_H q_v}{Dt} - G_u \frac{L_d}{L} w = 0, \tag{9c}$$

and are closed by the balance relations

$$\zeta = \nabla_H^2 \psi, \quad u = -\frac{\partial \psi}{\partial y}, \quad v = \frac{\partial \psi}{\partial x}, \quad b_u = \theta = \frac{L}{L_d} \frac{\partial \psi}{\partial z}, \tag{10}$$

where $\frac{D_H}{Dt} = \frac{\partial}{\partial t} + J(\psi, \cdot)$ is the horizontal material derivative, $J(\psi, \varphi) = (\partial\psi/\partial x)(\partial\varphi/\partial y) - (\partial\varphi/\partial x)(\partial\psi/\partial y)$ is the determinant of the Jacobian, ∇_H^2 is the horizontal Laplacian, L is a horizontal reference scale, $L_d^2 = (g/\theta_0)(d\tilde{\theta}/dz)H^2/f^2$ is the deformation radius of dry dynamics for a reference height H, and $G_u = -(L_v/c_p)(d\tilde{q}_v/dz)/(d\tilde{\theta}/dz)$ is an unsaturated vertical moisture gradient ratio. As in the standard QG setup, due to geostrophic and hydrostatic balance, the pressure acts as a stream function ψ which relates all dynamical variables. To obtain the system (9a)–(9c), we have chosen the following distinguished limit:

$$\begin{aligned} &\mathrm{Ro}\,\mathrm{Eu} = 1, \quad \Gamma A^2 = Fr_u^{-1}, \quad Fr_u = \frac{L}{L_d}\mathrm{Ro}, \\ &\frac{L_d}{L} = O(1), \quad G_u = O(1), \quad \frac{gQ}{B} = O(\mathrm{Ro}), \end{aligned} \tag{11}$$

valid in the small Rossby number limit, where $\mathrm{Ro} = U/(fL)$ is the Rossby number, $\mathrm{Eu} = P/(\rho_0 U^2)$ is the Euler number, Fr_u is the unsaturated Froude number, $\Gamma = BH/W^2$ is a buoyancy parameter, and $A = H/L$ is the aspect ratio. Note that the relations in (11) imply that equations (9b)–(9c) correspond to (7) when dimensionalized if the material derivative is replaced with the horizontal material derivative.

One interesting aspect of the equations obtained here lies in the fact that, to first-order correction, the unsaturated buoyancy is merely the 'dry' buoyancy; see (10) and note that conditions (11) reduce the bouyancy equation (8) simply into equation (7) for the potential temperature in the small Rossby limit. Thus, in the small Rossby limit, the nonlinear dynamics given by (9a), (9b), (10) in the unsaturated regions are identical to those of the dry regions. Namely, the background state water vapor $\tilde{q}_v$ and anomaly water vapor q_v do not affect the evolution of the winds, potential temperature, and pressure in the unsaturated regime of the PQG model. This is not a feature of the FARE system itself, but rather arises in the QG limit from the small relative contribution that moisture has on the unsaturated buoyancy. As a consequence, water vapor anomaly in unsaturated regions must act as a passive tracer in the unsaturated regime. The background state of water vapor $\tilde{q}_v$ does, however, affect the advection of the water vapor anomaly; note parameter G_u in equation (9c).

2.3 PQG Equations in the Saturated Regime

Similarly, we specify the decomposition of the thermodynamic variables into a background anelastic state and anomaly when the dynamics are saturated; equation (4b). We suppose that our background state consists of known saturated functions $\tilde{q}_v$, $\tilde{q}_r$ and deviations from these background states never become unsaturated; namely, $\tilde{q}_v = \tilde{q}_{vs}$, $q_v = 0$, $\tilde{q}_r > 0$, and $q_r > -\tilde{q}_r$. In addition, we require that $d\tilde{q}_r/dz = 0$ to ensure a steady-state background profile; the case $V_T = 0$ is briefly discussed in Section 4.2.

In the saturated regime, the buoyancy (2) becomes

$$b_s = b(\theta, q_r) = g\left(\frac{\theta}{\theta_0} - q_r\right). \tag{12}$$

Therefore, in a saturated state, the relevant thermodynamic variables are the rainwater q_r and the potential temperature θ. As in the unsaturated case, we obtain a separation between background and anomalies of the form:

$$\begin{bmatrix} \tilde{\theta}_e \\ \tilde{q}_t \end{bmatrix} = \begin{bmatrix} 1 & 0 \\ 0 & 1 \end{bmatrix} \begin{bmatrix} \tilde{\theta} \\ \tilde{q}_r \end{bmatrix} + \begin{bmatrix} \frac{L_v}{c_p} \\ 1 \end{bmatrix} \tilde{q}_{vs} \quad \text{and} \quad \begin{bmatrix} \theta_e \\ q_t \end{bmatrix} = \begin{bmatrix} 1 & 0 \\ 0 & 1 \end{bmatrix} \begin{bmatrix} \theta \\ q_r \end{bmatrix}. \tag{13}$$

Then, the thermodynamic equations (3c)–(3d) of the FARE model become

$$\frac{D\theta}{Dt} + w\frac{d\tilde{\theta}_e}{dz} = 0 \quad \text{and} \quad \frac{Dq_r}{Dt} + w\frac{d\tilde{q}_t}{dz} = V_T\frac{\partial q_r}{\partial z}. \tag{14}$$

The equations in (14) may, again, be combined to form an equation for the buoyancy (12) in the saturated regime:

$$\frac{Db_s}{Dt} + wN_s^2 = -gV_T\frac{\partial q_r}{\partial z}, \tag{15}$$

where

$$N_s^2 = g\left(\frac{1}{\theta_0}\frac{d\tilde{\theta}_e}{dz} - \frac{d\tilde{q}_t}{dz}\right) = g\left(\frac{1}{\theta_0}\frac{d\tilde{\theta}}{dz} - \frac{d\tilde{q}_r}{dz} + \left(\frac{L_v}{c_p\theta_0} - 1\right)\frac{d\tilde{q}_{vs}}{dz}\right). \tag{16}$$

By similar manipulations to those in the unsaturated case, under the non-dimensionalization shown in Table 3, it is possible to show that the evolution of non-dimensional first-order correction quantities in the small Rossby limit give the equations [27]

$$\frac{D_H\zeta}{Dt} = \frac{\partial w}{\partial z}, \tag{17a}$$

$$\frac{D_H b_s}{Dt} + \frac{L_{de}}{L}w = 0, \tag{17b}$$

$$\frac{D_H q_r}{Dt} - G_s\frac{L_{de}}{L}w = V_r\frac{\partial q_r}{\partial z}, \tag{17c}$$

which are closed by the balance relations

$$\zeta = \nabla_H^2\psi, \quad u = -\frac{\partial\psi}{\partial y}, \quad v = \frac{\partial\psi}{\partial x}, \quad b_s = \theta = \frac{L}{L_{de}}\frac{\partial\psi}{\partial z}, \tag{18}$$

where $V_r = V_T/W$ is the non-dimensional precipitation velocity, L is a horizontal reference scale, $L_{de}^2 = (g/\theta_0)(d\tilde{\theta}_e/dz)H^2/f^2$ is the moist deformation radius, and $G_s = -(L_v/c_p)(d\tilde{q}_t/dz)/(d\tilde{\theta}_e/dz)$ is a saturated vertical moisture gradient ratio. To derive these equations, it is assumed that:

$$\begin{gathered} \text{Ro Eu} = 1, \quad \Gamma A^2 = Fr_s^{-1}, \quad Fr_s = \frac{L}{L_{de}}\text{Ro}, \\ \frac{L_{de}}{L} = O(1), \quad G_s = O(1), \quad V_r = O(1), \quad \frac{gQ}{B} = O(\text{Ro}), \end{gathered} \tag{19}$$

in the small Rossby number limit, where Fr_s is the saturated Froude number; an alternative limiting scenario of $V_r \to \infty$ is discussed in [27]. As before, the relations in (19) imply that equations (17b)–(17c) correspond to (14) when dimensionalized if the material derivative is replaced with the horizontal material derivative.

A remarkable feature of these equations, which is shared with the unsaturated PQG equations, is that the first-order correction buoyancy in (18) does not have a moisture contribution and is only related to the potential temperature. Even though the non-linear equations for saturated dynamics are not identical to those in the dry regions, they fall into the same family of equations as those of the dry dynamics; replace parameter L_{de} with L_d. The dynamics in saturated regions are thus closed and, as in the unsaturated case, rainwater/moisture anomaly acts as a passive tracer if no phase change is allowed. Unlike the unsaturated regions, however, the chosen background moisture content of saturated regions – $\tilde{q}_{vs}$ in this case – affects the evolution of the winds, potential temperature, and pressure.

The fact that the dynamics of the PQG model are independent from the evolution of moisture originates from our representation of latent heating. This latent heating term is proportional to w only, which allows the dynamics to evolve unaffected by the moisture evolution; note that the equation (14) can be written as

$$\frac{D\theta}{Dt} + w\frac{d\tilde{\theta}}{dz} = -w\frac{L_v}{c_p}\frac{d\tilde{q}_{vs}}{dz}, \tag{20}$$

where the right-hand side term is the latent heating arising in the saturated regime. However, if we had chosen or obtained a representation of the latent heating depending directly on a moisture variable, say, q_t or q_r, no such decoupling would take place. The interested reader is referred to Smith and Stechmann [27] for further discussion on this separation.

3 Linear Instability Analysis: Eady Problem

In this section, we study the effect that moisture has on the linear stability of the PQG equations by solving the 'Eady problem'. Namely, we study the linear stability properties of the normal mode solutions of the PQG system about a uniform vertical background zonal velocity shear which is unstable. This serves as possibly the simplest case to test the linear stability properties of the PQG system and glean some understanding on the parameter dependence for the flow's stability. There are many derivations of the Eady problem for 'dry' dynamics (dry regime) that can be found in the standard sources [7, 15, 24, 30, to name a few]. The derivation here is analogous to the dry case since the equations of the dynamics of PQG are completely unaffected by the moisture anomaly and are only affected by background moisture in the saturated regime. For completeness and aid of exposition, we provide a full derivation here and accentuate certain aspects of the derivation which are relevant to understand the dependence on the parameter L_d or L_{de}. The solutions in this section will form the basis for the investigation of water transport in Section 4.

3.1 Derivation of the Solution

We begin by constructing a potential vorticity equation from the PQG equations in the unsaturated and saturated regimes. Namely, equations (9a)–(9b) in unsaturated regimes and (17a)–(17b) in saturated regimes may be combined as is usual in 'dry' QG to obtain an equation without the effects of the vertical velocity in the interior of the domain. This gives an equation for the conservation of potential vorticity P:

$$\frac{D_H P}{Dt} = 0 \quad \text{for } 0 \le z \le 1, \tag{21}$$

where

$$P = \nabla_H^2 \psi + \frac{L^2}{L_D^2}\frac{\partial^2 \psi}{\partial z^2}, \quad u = -\frac{\partial \psi}{\partial y}, \quad v = \frac{\partial \psi}{\partial x}, \qquad \text{and} \quad b = \frac{L}{L_D}\frac{\partial \psi}{\partial z}. \tag{22}$$

Here L_D denotes the relevant deformation radius of the problem at hand, i.e., $L_D = L_d$ in dry/unsaturated regimes and $L_D = L_{de}$ in saturated regimes. In addition, we impose a 'rigid lid' ($w = 0$) boundary condition on the top and bottom boundaries of the flow. To accomplish this, we directly evaluate the buoyancy equations (9b) and (17b) at the boundaries $z = 0, 1$, which gives an evolution equation for the buoyancy at the vertical boundaries:

$$\frac{D_H b}{Dt} + \frac{L_D}{L} w = 0 \quad \text{for } 0 \le z \le 1 \text{ with } w = 0 \text{ at } z = 0, 1. \tag{23}$$

To study the linear stability of the PQG equations, we consider the perturbations about the background flow consisting of a constant shear Λz in the zonal direction for some constant $\Lambda > 0$ on $0 \le z \le 1$. Then, equations (21) and (23) become the linearized equations for potential vorticity P and buoyancy b perturbation – subject to this background state –

$$\left(\frac{\partial}{\partial t} + \Lambda z \frac{\partial}{\partial x}\right) P = 0 \quad \text{for } 0 \le z \le 1, \tag{24a}$$

$$\left(\frac{\partial}{\partial t} + \Lambda z \frac{\partial}{\partial x}\right) b - \frac{L}{L_D}\Lambda \frac{\partial \psi}{\partial x} + \frac{L_D}{L} w = 0 \quad \text{for } 0 \le z \le 1 \tag{24b}$$

with $w = 0$ at $z = 0, 1$, and the streamfunction satisfying (22). Note that the $\partial\psi/\partial x$ term in (24b) arises from the $v\,\partial b/\partial y$ term of the original buoyancy equation in (23). In addition, the parameter $L\Lambda/L_D$ may be understood in terms of the Rossby number Ro and Richardson number $\mathrm{Ri} = N^2/(dU/dz)^2$, where N is the relevant buoyancy frequency and dU/dz is the vertical velocity gradient; namely, $L\Lambda/L_D = \mathrm{Ro}^{-1}\mathrm{Ri}^{-1/2}$.

To describe the stability of the solutions of the system (24a) and (24b), we may obtain the dispersion $\omega = \omega(k, l)$ relation by seeking normal mode solutions. The doubly periodic normal mode solutions are

$$\psi = \mathrm{Re}\{\Psi(z) e^{i(kx+ly-\omega t)}\} \quad \text{and} \quad w = \mathrm{Re}\{W(z) e^{i(kx+ly-\omega t)}\} \tag{25}$$

and the normal mode solutions in a channel of (dimensional) width L_c with boundaries $y = -L_c/(2L), L_c/(2L)$ are

$$\psi = \mathrm{Re}\{\Psi(z)\cos(ly)e^{i(kx-\omega t)}\} \quad \text{and} \quad w = \mathrm{Re}\{W(z)\cos(ly)e^{i(kx-\omega t)}\}, \tag{26}$$

where $l = (2n+1)\pi L/L_c$ for any positive integer n; recall that y has been non-dimensionalized by the reference horizontal scale L which is taken to be of a size comparable to the deformation radius L_D. The subsequent analysis of the doubly periodic and channel normal modes is much the same, so we combine it here and state the salient differences when they arise.

Substituting the normal mode ansatz (25) or (26) into the equations (24a)–(24b) with (22) we obtain

$$(C-z)\left(-\mu_\kappa^2\Psi + \frac{d^2\Psi}{dz^2}\right) = 0 \quad \text{for } 0 \le z \le 1, \tag{27a}$$

$$(C-z)\frac{d\Psi}{dz} + \Psi + \frac{i}{k\Lambda}\left(\frac{L_D}{L}\right)^2 W = 0 \quad \text{for } 0 < z < 1, \tag{27b}$$

$$(C-z)\frac{d\Psi}{dz} + \Psi = 0 \quad \text{for } z = 0, 1, \tag{27c}$$

where we define the normalized phase speed $C = \omega/(k\Lambda)$ and $\mu_\kappa^2 = \kappa^2 L_D^2/L^2$ for the wavenumber magnitude $\kappa^2 = k^2 + l^2$. Since L_D is taken to be a constant, it is straighforward to show that equation (27a) has a general solution of the form

$$\Psi(z) = c_1\cosh(\mu_\kappa z) + c_2\sinh(\mu_\kappa z). \tag{28}$$

The free constants c_1, c_2 are then chosen so that the solution (28) satisfies the boundary condition (27c):

$$\begin{bmatrix} 1 & \mu_\kappa C \\ (C-1)\mu_\kappa\sinh\mu_\kappa + \cosh\mu_\kappa & (C-1)\mu_\kappa\cosh\mu_\kappa + \sinh\mu_\kappa \end{bmatrix}\begin{bmatrix} c_1 \\ c_2 \end{bmatrix} = \begin{bmatrix} 0 \\ 0 \end{bmatrix}. \tag{29}$$

The system (29) has a nontrivial solution (c_1, c_2) when the determinant of the system is identically zero, i.e.,

$$C_\pm = C_\pm(\mu_\kappa) = \frac{1}{2} \pm \frac{1}{2\mu_\kappa}\sqrt{\left(\mu_\kappa - 2\tanh\frac{\mu_\kappa}{2}\right)\left(\mu_\kappa - 2\coth\frac{\mu_\kappa}{2}\right)}. \tag{30}$$

Thus, instability for the normal mode solutions only arises from the C_+ branch of the phase speed and, since moisture anomaly does not contribute to the dynamics, no additional unstable modes arise due to moisture; in contrast to Lambaerts et al. [17] and Monteiro and Sukhatme [21]. The unstable solutions to the Eady problem are given by

$$\Psi(z) = c_1\Psi_1(z), \quad \text{where} \quad \Psi_1(z) = \cosh(\mu_\kappa z) - \frac{\sinh(\mu_\kappa z)}{\mu_\kappa C_+(\mu_\kappa)} \tag{31}$$

for any free constant c_1.

3.2 Instability Growth Rate

The Eady Problem is linearly unstable when the discriminant of equation (30) is negative, i.e.,

$$\frac{\mu_\kappa}{2} < \coth\frac{\mu_\kappa}{2} \quad \text{or} \quad 0 \le \mu_\kappa < \mu_c, \tag{32}$$

where $\mu_c \approx 2.39936$. In particular, this implies that wavenumbers leading to instability satisfy

$$0 \le \sqrt{k^2+l^2} < \mu_c\frac{L}{L_D}\ \text{(non-dim.)} \quad \text{or} \quad 0 \le \sqrt{k^2+l^2} < \mu_c\frac{1}{L_D}\ \text{(dim.)}, \tag{33}$$

where "non-dim." denotes non-dimensional and "dim." denotes dimensional. So that if L_D is increased (decreased), the wavenumber region of instability is reduced (expanded) to lower (higher) wavenumbers; see Figure 1. Therefore, including moisture into the system, with its effect of reducing the relevant deformation

radius L_D, will lead to the instability affecting smaller scale waves than in the equivalent 'dry' problem. Specifically, the length scales λ associated with the greatest instability are

$$\lambda = \frac{2\pi}{Lk_m} = \frac{2\pi L_D}{L\mu_m} \approx 3.91\frac{L_D}{L} \text{ (non-dim.)} \quad \text{or} \quad \lambda \approx 3.91 L_D \text{ (dim.)}. \tag{34}$$

As stated in most sources of the 'dry' Eady problem [e.g., 15, 24, 30], the maximum growth rate Im $\omega = \sigma_m$ is obtained at the wavenumber determined by $\mu_m \approx 1.60612$ with $C_+(\mu_m) \approx 0.5 + 0.192898i$. As in the dry dynamics, the growth rate of the most unstable mode is greatest when the wavenumber in the meridional direction l is the smallest possible; $l = 0$ for the doubly periodic case and $l = \pi L/L_c$ in the channel case. Below we will show results with $l = 0$, which may still be appropriate for the channel case if the channel's width is larger than the deformation radius of the problem ($L_c \gg L_D \sim L$).

Then, the most unstable growth rate σ_m ($\mu_m \approx 1.60612$ with $l = 0$) is

$$\sigma_m = k\Lambda \text{ Im}\{C_+(\mu_m)\} \approx 0.31\frac{L\Lambda}{L_D} \text{ (non-dim.) or } \sigma_m \approx 0.31\frac{U\Lambda}{L_D} \text{ (dim.)}, \tag{35}$$

where U is the reference horizontal velocity with which Λ is non-dimensionalized. Equivalently, we may write the growth rate in terms of the Richardson number as $\sigma_m \approx 0.31 f_0 \text{Ri}^{-1/2}$. Thus, the growth rate increases as L_D^{-1} if L_D is made smaller by the addition of moisture (Figure 1). This is consistent with the broad conclusions of Bannon [2], Emanuel et al. [8], Lambaerts et al. [17], Lapeyre and Held [18], Mak [19] who observed that the addition of moisture increases the growth rate of the instability.

These results on the growth rate and length scales of the most unstable Eady modes are completely standard and expected from 'dry' Eady problem theory if we interpret the dry deformation radius as a moisture parameter. It is of interest, however, that these results arise in this study strictly from asymptotic analysis of the FARE model and linear instability theory and not by assuming that moist static stability is applicable a priori to the Eady problem.

We may briefly use the concept of moist static stability to compare these results on growth rates using known data. In a careful study, O'Gorman [22] showed that the ratio between moist static stability and dry stability (L_{de}^2/L_d^2 in our paper) may vary significantly in mid-latitudes from a lowest value of ≈ 0.5 in the low troposphere to ≈ 0.9 in the upper troposphere. Taking the value $L_{de}^2/L_d^2 \approx 1/2$, we obtain an increase in the moist instability growth rate of 41% ($L_d/L_{de} \approx \sqrt{2} \approx 1.41$) in comparison to the dry/unsaturated growth rate. Using the same value, in a numerical simulation about a background jet of a two-layer shallow-water model Lambaerts et al. [17] found that (in the initial stages of instability) the instability growth rate increased by about 32% from the value in the dry case once moisture effects become significant. Similarly, in a numerical study of baroclinic waves using a hydrostatic spectral model on a sphere (all ascending air assumed to be saturated while all descending air is assumed to be dry), Govindasamy and Garner [12] showed that the moist growth rate being about 45% larger than that in the dry case. These comparisons suggest that the overall growth rate changes are captured by the simple Eady model.

We may additionally quantify the effect of moisture by estimating realistic values of $d\tilde{\theta}/dz$ and $d\tilde{q}_{vs}/dz$ directly. We may do so crudely by using Figures 5.8 and 5.16 of Marshall and Plumb [20] to obtain the estimates $d\tilde{\theta}/dz \approx 3$ K km^{-1} and $d\tilde{q}_{vs}/dz \approx -0.8$ g kg^{-1} km^{-1}. For these values, $L_d \approx 990$ km for dry/unsaturated regimes and $L_{de} \approx 572$ km for saturated regimes, we find

$$\begin{aligned} \text{Dry/Unsaturated regimes: } \sigma_m &\approx 0.27\Lambda \text{ day}^{-1} \quad \text{and} \quad \lambda \approx 3,873 \text{ km} \\ \text{Saturated regimes: } \sigma_m &\approx 0.47\Lambda \text{ day}^{-1} \quad \text{and} \quad \lambda \approx 2,236 \text{ km}. \end{aligned} \tag{36}$$

This in turns implies that the moist growth rate is $(0.47\Lambda)/(0.27\Lambda) \approx 1.74$ times larger than the dry growth rate. A similar value of $1.15/0.67 \approx 1.72$ was found by Gall [11] using numerical simulations of a primitive equation model with latent heat release. In contrast to these Eady problem results, however, Gall [11] also found that the wavelength of greatest instability in his model is unaffected by moisture.

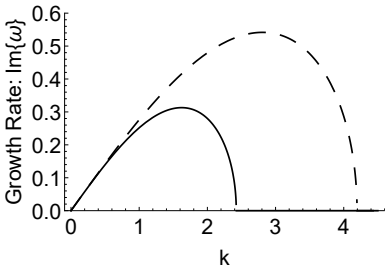

Figure 1: Dimensionless growth rate $\sigma = \mathrm{Im}\{\omega\}$ as a function of the zonal wavenumber k for the dry/unsaturated regime (solid curve; $L_D = L_d \approx 990$ km) and saturated regime (dashed curve; $L_D = L_{de} \approx 572$ km).

3.3 Normalization of the Normal Modes

To compare the effects of moisture on our linear solutions, here and in the rest of the paper, we normalize the streamfunction (31) so that the initial total (kinetic plus dry potential) energy of the system is equal to unity; refer to Appendix A for a discussion on the normalization of the normal modes. This implies

$$c_1 = \frac{L_D}{L}\frac{1}{\sqrt{\epsilon_\mu}}, \quad \text{where } \epsilon_\mu = \frac{1}{4}\int_0^1 \left(\mu_\kappa^2 \Psi_1(z)\Psi_1^\star(z) + \frac{d\Psi_1^\star}{dz}(z)\frac{d\Psi_1}{dz}(z)\right) dz \tag{37}$$

and $\varphi^\star$ denotes the complex conjugate of φ. Note that ϵ_μ is merely a function of μ_κ, so that the parameter dependence of the norming constant c_1 in (37) on L_D/L is explicit. Namely, the effects of moisture on the streamfunction are explicitly given in this normalization of the streamfunction by the constant c_1 since L_D contains all the (background) moisture information which may affect the dynamics. Here onward Ψ will denote the streamfunction (31) with the normalization (37).

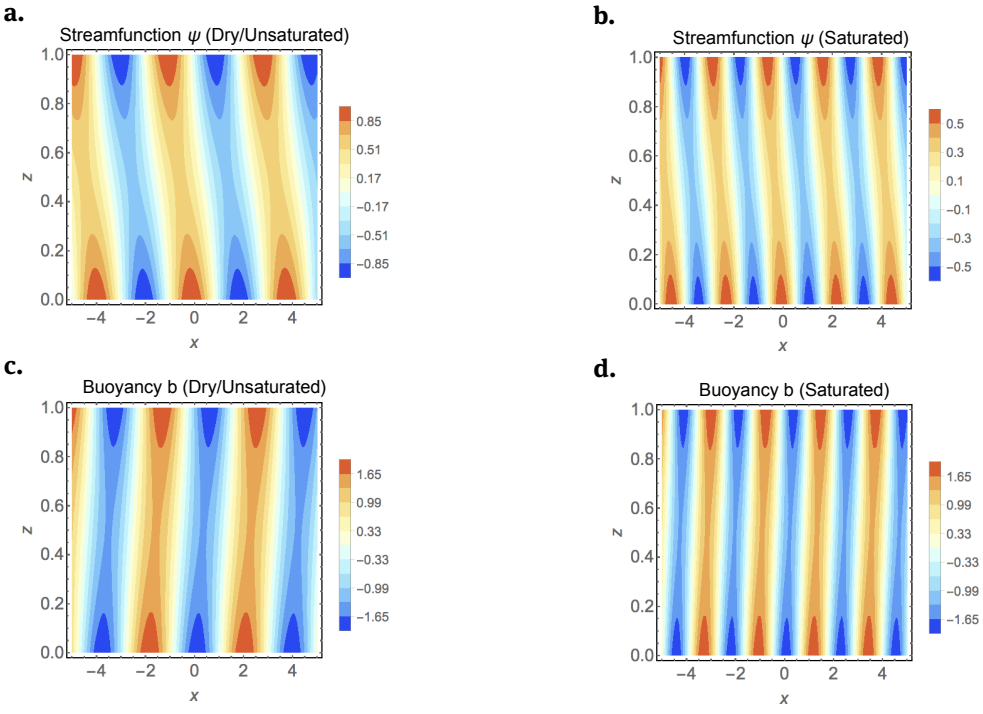

Figure 2: Structure of the most unstable normal modes for the streamfunction (panels **a.** and **b.**) and buoyancy (panels **c.** and **d.**) of the Eady problem. Panels **a.** and **c.**: dry/unsaturated regime $L_D = L_d \approx 990$ km. Panels **b.** and **d.**: saturated regime $L_D = L_{de} \approx 572$ km.

Under the normalization (37), the dependence of the streamfunction ψ and buoyancy b on the moisture parameter L_D is easily discerned. For the most unstable mode, the length scales of all variables are proportional to L_D; since $k \propto L_D^{-1}$. That is, addition of moisture (in the form of L_D) into the problem will merely decrease the length scales while keeping the shape of the structures the same. In the case of the streamfunction ψ, the amplitude also scales with L_D. Thus, all else held equal, pressure (streamfunction) disturbances are attenuated and contracted by the addition of moisture. The amplitude of the buoyancy, in contrast, is independent of the background moisture. This is intuitively sensible since the buoyancy in the PQG context is simply the potential temperature and should be independent of the moisture parameter L_D. Lastly, the zonal and meridional velocities u, v also have amplitudes independent of the moisture content. See Figure 2 for a representation of the structures of the streamfunction and buoyancy in the Eady problem for different, physically relevant, values of L_D.

3.4 Heat Fluxes

To contrast with the water fluxes that will be studied in Section 4, we now derive formulas for the meridional heat flux, $\langle vb \rangle$, where

$$\langle \varphi \rangle := \frac{k}{2\pi} \int_0^{2\pi/k} \varphi(x)\, dx \tag{38}$$

denotes the zonal mean over one period in x.

The dependence of the meridional flux on L_D is not readily discernible in general. However, this dependence simplifies significantly when considering the most unstable wavenumber $(k, l) \approx (\mu_m/L_D, 0)$. For this most unstable mode, we have observed in Section 3.3 that the amplitudes of both the meridional velocity v and potential temperature b are independent of the parameter L_D (they are unaffected by moisture content). By direct computation, the meridional heat flux – using the zonal mean result in Appendix B and (27a), (27c) – is

$$\langle vb \rangle = \frac{1}{2} \mathrm{Re} \left\{ ik\Psi(z) B^\star(z) \right\} = \mathcal{B}_\mu(0) e^{2\sigma_m t} \tag{39}$$

in the doubly periodic case and

$$\langle vb \rangle = \cos^2(ly) \mathcal{B}_\mu(0) e^{2\sigma_m t} \tag{40}$$

in the channel case (σ_m is the largest growth rate), where

$$\mathcal{B}_\mu(z) = \frac{1}{2\epsilon_\mu} \left(\mu_\kappa^2 - \frac{L_D^2}{L^2} l^2 \right)^{1/2} \mathrm{Im}\{C\} \left| \frac{d\Psi_1}{dz} \right|^2 (z). \tag{41}$$

To obtain the result (39) and (40), we have used the following identity arising from equations (27a) and (27c):

$$\mathrm{Re} \left\{ i\Psi \frac{d\Psi^\star}{dz} \right\} = \mathrm{Im}\{C\} \left| \frac{d\Psi}{dz} \right|^2 (0) = \mathrm{Im}\{C\} \left| \frac{d\Psi}{dz} \right|^2 (1). \tag{42}$$

Note that for the most unstable wavenumber (assuming that $L_c \gg L$ in channel mode case), the function $\mathcal{B}_\mu$ in (41) is a function of only μ_κ and is independent of L_D; see Figure 3. Thus, the meridional heat flux is unchanged by the addition of moisture or changes in the moisture content. Moreover, the flux is positive and independent of z, so that net heat transport is northward and uniform across the air column; see Figure 4.

4 Water Transport

Our analysis of the transport of moisture follows the same basic procedure as the analysis of heat transport, i.e., we use the normal mode solutions to discern the dependence of water transport on the background moisture. The relevant moisture parameters for water transport are the vertical water gradient, meridional water

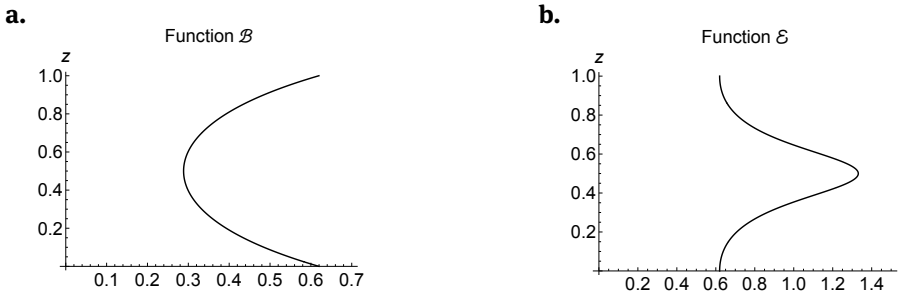

Figure 3: Graph of $\mathcal{B}_\mu(z)$ (panel **a.**) and $\mathcal{E}_\mu(z)$ (panel b.) for most unstable wavenumber $\mu \approx 1.606$. The functions $\mathcal{B}_\mu$, $\mathcal{E}_\mu$ are independent of the deformation radius L_d and moisture parameters.

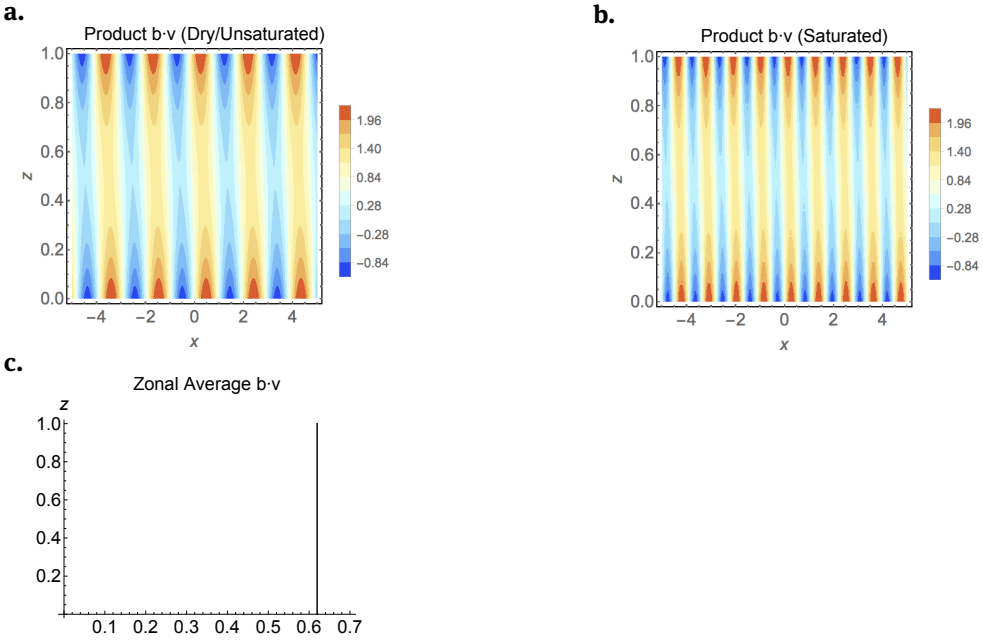

Figure 4: Product of the buoyancy b and meridional velocity v (Panel **a.**: dry/unsaturated regime $L_D = L_d \approx 990$ km; Panel **b.**: saturated regime $L_D = L_{de} \approx 572$ km) and zonal average of the meridional flux of buoyancy $\langle vb \rangle$ (Panel **c.**). Note that the flux is independent of chosen value of L_D except for the horizontal scale.

gradient, and rainfall speed (saturated phase only). In this section, we analyze both water vapor and rainwater fluxes and derive formulas with explicit moist parameter dependence. Due to the fact that our study is single-phase only, we treat unsaturated and saturated cases separately.

4.1 Unsaturated Regime

Here we discuss the derivation of the water vapor and subsequently the meridional flux from the Eady normal modes. To begin, we choose a purely meridional background water vapor of the form $-\overline{Q}_v y$ (with $\overline{Q}_v \geq 0$ so that the background moisture decreases with latitude). A back-of-the-envelope calculation from Figure 5.15 of [20] suggests a sensible value to be $\overline{Q}_v^{dim} = 1/6$ g kg^{-1} degree^{-1} (dimensional), where

$$\overline{Q}_v = \overline{Q}_v^{dim} \frac{L_v}{c_p} \frac{L}{\Theta} \approx 1.25. \tag{43}$$

Linearizing about this chosen moisture background state and the Eady background state, equation (9c) becomes

$$\left(\frac{\partial}{\partial t} + \Lambda z \frac{\partial}{\partial x}\right) q_v - \overline{Q}_v \frac{\partial \psi}{\partial x} - G_u \frac{L_d}{L} w = 0. \tag{44}$$

For normal mode solutions of the form (25)–(26) with

$$q_v = \mathrm{Re}\{Q_v(z) e^{i(kx+ly-\omega t)}\} \quad \text{or} \quad q_v = \mathrm{Re}\{Q_v(z)\cos(ly) e^{i(kx-\omega t)}\} \tag{45}$$

in the doubly periodic and channel cases, respectively, equation (44) becomes

$$Q_v = -\frac{\overline{Q}_v}{\Lambda} \frac{\Psi}{(C-z)} + \frac{i}{k\Lambda} G_u \frac{L_d}{L} \frac{W}{(C-z)} \quad \text{for } 0 \le z \le 1, \tag{46}$$

where (as before) $C = \omega/(k\Lambda)$. We may equivalently substitute the vertical velocity term for the streamfunction, using (27b), to obtain

$$Q_v = -\frac{\overline{Q}_v}{\Lambda} \frac{\Psi}{(C-z)} - G_u \frac{L}{L_d} \left(\frac{d\Psi}{dz} + \frac{\Psi}{(C-z)}\right) \quad \text{for } 0 \le z \le 1. \tag{47}$$

Note that in the region of instability $C - z \neq 0$ and may freely divide by this term. The fact that $C - z \neq 0$ follows from the fact that the flow is unstable when C is a complex number and $0 \le z \le 1$ is always real.

The effect of moisture, in the form of meridional and vertical gradients of background water, on the water vapor may be immediately gleaned from equation (47). Specifically, since the streamfunction Ψ is independent of these moisture parameters, the net effect of background moisture on the water vapor may then be understood from the relative strength of the two competing terms in equation (47). For this reason, we see each term of (47) as contributing to a particular limiting case arising from the moisture gradient. In the case of strong meridional gradient of moisture ($\overline{Q}_v/\Lambda \gg G_u L/L_d$), we find that the water vapor is proportional to the meridional gradient $\overline{Q}_v$. Similarly, in the case of a weak meridional gradient ($\overline{Q}_v/\Lambda \ll G_u L/L_d$), the water vapor is proportional to the vertical gradient of moisture $d\tilde{q}_v/dz$; recall that $G_u = -(L_v/c_p)(d\tilde{q}_v/dz)/(d\tilde{\theta}/dz)$.

We may crudely estimate the value of vertical gradient of background moisture to be $d\tilde{q}_v/dz \approx -1.3$ g kg^{-1} km^{-1} from Figures 5.15 of Marshall and Plumb [20]. This provides a physically motivated estimate for the moisture parameter G_u to be $G_u \approx 1.08$ (recall $d\tilde{\theta}/dz \approx 3$ K km^{-1}). For the value $G_u \approx 1.08$ and our other chosen moisture parameters, we find that neither term in (47) dominates; moderate meridional gradient of background moisture. Using these parameters, we show numerically the effect that the background moisture has on the structure of the water vapor in Figure 5. We note from Figure 5 that the addition of the meridional gradient of moisture slightly stretches each cell of water vapor vertically and significantly increases each cell's amplitude. In this manner, more water vapor is present at the vertical boundaries of the domain.

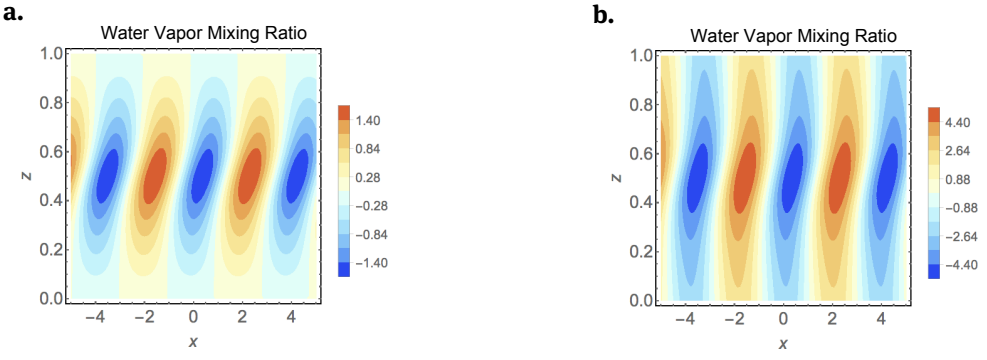

Figure 5: Structure of the most unstable mode of the water vapor q_v. Panel **a.**: $\overline{Q}_v = 0$ (no background meridional moisture gradient). Panel **b.**: $\overline{Q}_v = 1.25$ (moderate background meridional moisture gradient).

The meridional water vapor flux $\langle vq_v \rangle$ can similarly be obtained by direct computation, using the zonal mean result in Appendix B and (27a), (27c), (31), and (37):

$$\langle vq_v \rangle = \left(G_u \left(\mathcal{E}_\mu(z) - \mathcal{E}_\mu(0) \right) + \frac{L_d}{L} \frac{\overline{Q}_v}{\Lambda} \mathcal{E}_\mu(z) \right) e^{2\sigma_m t} \tag{48}$$

and

$$\mathcal{E}_\mu(z) = \frac{1}{2\epsilon_\mu} \left(\mu_\kappa^2 - \frac{L_d^2}{L^2} l^2 \right)^{1/2} \mathrm{Im}\{C\} \left| \frac{\Psi_1(z)}{C - z} \right|^2 . \tag{49}$$

As in the heat transport case, the key feature of the formula (48) is that for the most unstable wavenumber $(k, l) \approx (\mu_m / L_d, 0)$ the quantity $\mathcal{E}_\mu$ depends only on the universal fixed μ_κ, which is independent of the moisture content, and explicitly shows the contributions that background moisture has on the flux through the parameters G_u (vertical gradient of moisture) and $L_d \overline{Q}_v / (L\Lambda)$ (meridional gradient of moisture). Recall that $\mu = \mu_m \approx 1.60612$ for the most unstable mode and, also, $C \approx 0.5 + i0.192898$ – the phase speed – is fixed for a given μ_κ and the streamfunction Ψ_1 is determined by μ_κ.

We may interpret the meridional flux of water by noting that

$$\mathcal{E}_\mu(0) = \mathcal{E}_\mu(1) = \mathcal{B}_\mu(0) = \mathcal{B}_\mu(1) = |C|^{-2} \quad \text{and} \quad \mathcal{E}_\mu(z) \geq \mathcal{E}_\mu(0). \tag{50}$$

Therefore, since $L_d, L, \Lambda, \overline{Q}_v, G_u > 0$ there is always northward transport of water vapor, regardless of the parameter choices. Additionally, from Figure 3 we may deduce that the majority of this transport occurs at the center of the air column ($z = 1/2$) even though this is where the amplitude $k|\Psi(z)|$ of the meridional velocity is smallest; see, for example, Figure 2 which shows a minimum for $|\Psi(z)|$ at $z = 1/2$. In the case that there is no meridional water vapor gradient, $\overline{Q}_v = 0$, there is no net meridional water vapor transport at the top and bottom boundaries of the domain; $\langle vq_v \rangle = 0$ at $z = 0, 1$; see Figure 6. We may indeed understand the effects of moisture on the meridional flux of water simply by examining the strong $L_d \overline{Q}_v / (L\Lambda) \gg G_u$ and weak $L_d \overline{Q}_v / (L\Lambda) \ll G_u$ limits of the meridional gradient of moisture; in complete analogy to our result concerning the water vapor itself.

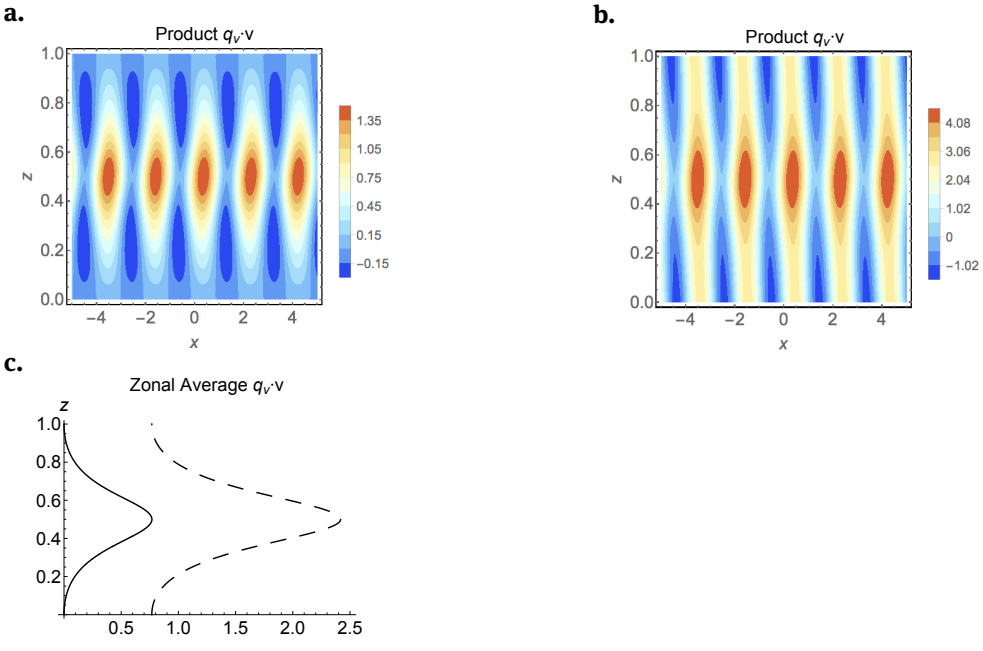

Figure 6: Product of water vapor q_v with meridional velocity v (Panel **a.**: $\overline{Q}_v = 0$; Panel **b.**: $\overline{Q}_v = 1.25$) and zonal average of the meridional flux of water vapor $\langle vq_v \rangle$ (Panel **c.**: Solid curve $\overline{Q}_v = 0$, dashed curve $\overline{Q}_v = 1.25$).

4.2 Saturated Regime

For saturated regimes, we choose a purely meridional background rainwater of the form $-\overline{Q}_r y$ ($\overline{Q}_r \geq 0$); in similar fashion to the background chosen in the unsaturated case. The linearization of the saturated equations is then analogous to that of the unsaturated equations and equation (17c) becomes

$$\left(\frac{\partial}{\partial t} + \Lambda z \frac{\partial}{\partial x}\right) q_r - \overline{Q}_r \frac{\partial \psi}{\partial x} - G_s \frac{L_{de}}{L} w = V_r \frac{\partial q_r}{\partial z}. \tag{51}$$

For normal mode solutions of the form (25)–(26) with

$$q_r = \mathrm{Re}\{Q_r(z) e^{i(kx+ly-\omega t)}\} \quad \text{or} \quad q_r = \mathrm{Re}\{Q_r(z)\cos(ly) e^{i(kx-\omega t)}\} \tag{52}$$

in the doubly periodic and channel cases, respectively, equation (51) becomes

$$-\frac{i}{k\Lambda} V_r \frac{dQ_r}{dz} + (C-z) Q_r + \frac{\overline{Q}_r}{\Lambda} \Psi - \frac{i}{k\Lambda} G_s \frac{L_{de}}{L} W = 0 \quad \text{for } 0 \leq z \leq 1. \tag{53}$$

We may similarly write (53) only in terms of the streamfunction by using (27b):

$$-\frac{i}{k\Lambda} V_r \frac{dQ_r}{dz} + (C-z) Q_r + \frac{\overline{Q}_r}{\Lambda} \Psi + G_s \frac{L}{L_{de}} \left((C-z)\frac{d\Psi}{dz} + \Psi\right) = 0 \quad \text{for } 0 \leq z \leq 1. \tag{54}$$

Thus, the condition $V_r = 0$ constitutes a singular limit of the equations (53)–(54) for the rainwater Q_r; see, for example, Appendix C for a brief discussion of this fact. As expected from our previous discussion, when $V_r = 0$ the equations of the rainwater Q_r are identical to those of the water vapor Q_v upon relabelling of the moisture parameters. The equations are, however, qualitatively and quantitatively different when $V_r \neq 0$.

An explicit solution for Q_r can be obtained from (54) in the case $V_r \neq 0$. Namely, using the boundary condition $Q_r(1) = 0$,

$$Q_r(z) = i\alpha e^{i\alpha(C-z)^2/2} \int_1^z e^{-i\alpha(C-\zeta)^2/2} \left(\frac{\overline{Q}_r}{\Lambda}\Psi(\zeta) + G_s \frac{L}{L_{de}} \left((C-\zeta)\frac{d\Psi}{d\zeta}(\zeta) + \Psi(\zeta)\right)\right) d\zeta, \tag{55}$$

where

$$\alpha = \frac{k\Lambda}{V_r} \quad \text{or} \quad \alpha = \frac{L}{L_{de}} \left(\mu_k^2 - \frac{L_{de}^2}{L^2} l^2\right)^{1/2} \frac{\Lambda}{V_r}. \tag{56}$$

The boundary condition $Q_r(1) = 0$ is chosen under the premise that rainwater should not precipitate from the top boundary.

From formula (55) it is clear that the dependence of rainwater on the background moisture parameters is not as simple as in the previous case of water vapor. Some understanding of this interaction can, however, be gleaned numerically using the default values of parameters discussed previously in the text (leading to $G_s = 0.67$); see Figures 7 and 8. We note that the addition of a meridional background moisture gradient changes the rainwater structure analogously to the unsaturated case: increasing $\overline{Q}_r$ significantly increases the magnitude of the rainwater and stretches each cell of rainwater in the vertical direction so that more/less rainwater is felt at the vertical boundaries of the domain. The addition of precipitation V_r (precipitation speed) into the problem concentrates the rainwater toward the lower boundary of the domain. Interestingly, this appears to be caused by a significant amount of rainwater not appearing in the center of the air column as it did in the case with $V_r = 0$; see Figure 8.

Formulas for the fluxes with explicit parameter dependence are only easily obtained in the case $V_r = 0$. Since, in this circumstance, the fluxes are equivalent to those in the unsaturated case with the relabeling $G_u \mapsto G_s$, $L_d \mapsto L_{de}$, $\overline{Q}_v \mapsto \overline{Q}_r$, we do not present them here. Rather, we focus on the case $V_r \neq 0$ and show results using plots for a range of parameter values.

A derivation for formulas of the meridional flux when $V_r \neq 0$ is more cumbersome than those in the unsaturated case. Nonetheless, the structure of the fluxes is analogous to those obtained for water vapor. Namely, there is an interplay between the strength of the meridional background $L_{de}\overline{Q}_r/(L\Lambda)$ and vertical

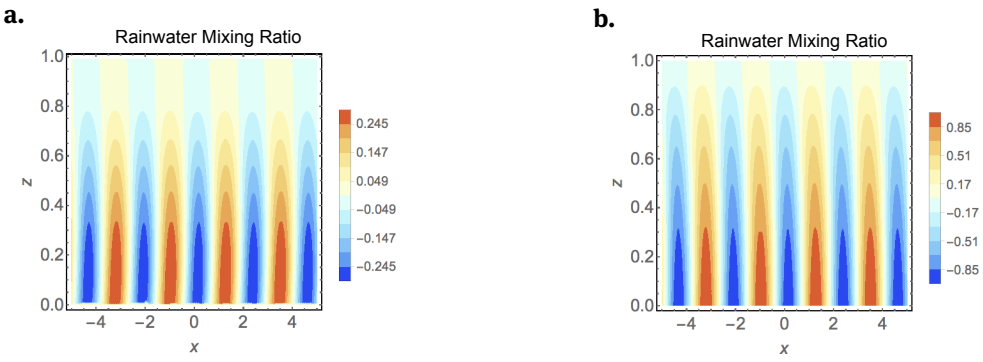

Figure 7: Structure of the most unstable rainwater mode q_r with and without background moisture gradient. Panel **a.**: $\overline{Q}_r = 0$, $V_r = 1$. Panel **b.**: $\overline{Q}_r = 1$, $V_r = 1$.

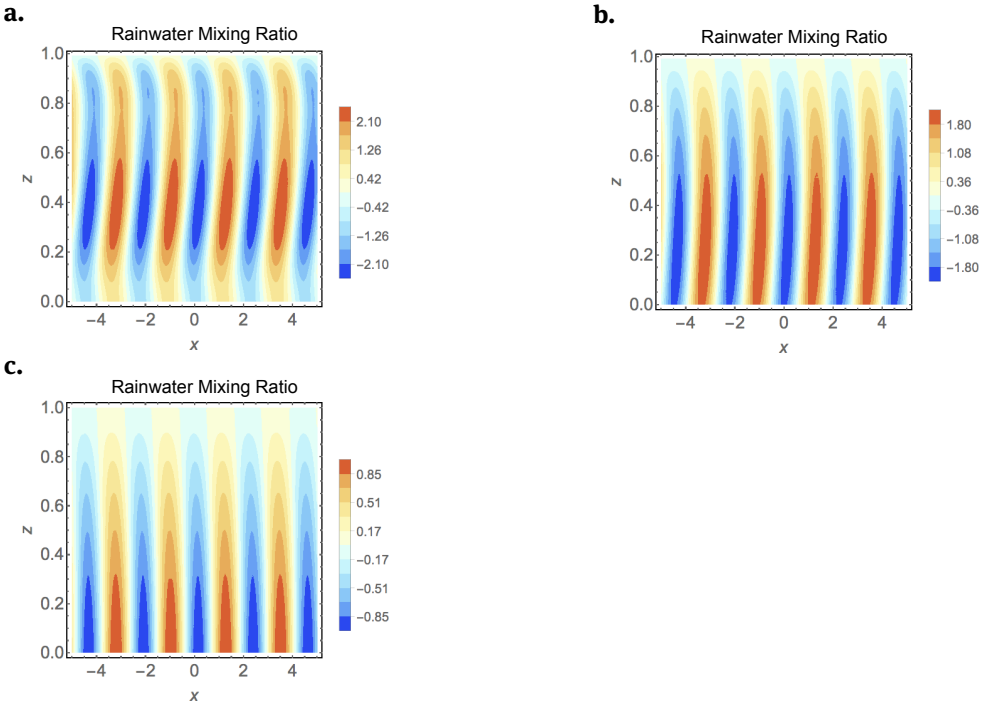

Figure 8: Structure of the most unstable rainwater mode q_r for different values of the rainfall speed. Panel **a.**: $\overline{Q}_r = 1$, $V_r = 1/16$. Panel **b.**: $\overline{Q}_r = 1$, $V_r = 1/4$. Panel **c.**: $\overline{Q}_r = 1$, $V_r = 1$.

background G_s of moisture. The moisture parameters L_{de} and V_r, on the other hand, have a significantly more complicated interaction with the rainwater. We may note from the plots below that the primary effect of the different structure of rainwater is that water, principally from lower in the air column, is moved northward by the meridional wind. Explicitly,

$$\langle vq_r \rangle = \frac{1}{2}\mathrm{Re}\left\{-ik\Psi^\star Q_r\right\} e^{2\sigma_m t} = \left(G_s G_\alpha(z) + \frac{\overline{Q}_r}{\Lambda}\frac{L_{de}}{L}F_\alpha(z)\right) e^{2\sigma_m t} \tag{57}$$

with functions

$$F_\alpha(z) = -\frac{\alpha}{2}\frac{\mu_\kappa}{\epsilon_\mu}\mathrm{Re}\left\{\Psi_1^\star(z)e^{i\alpha(C-z)^2/2}\int_1^z e^{-i\alpha(C-\zeta)^2/2}\Psi_1(\zeta)\,d\zeta\right\} \tag{58}$$

and

$$G_\alpha(z) = -\frac{\alpha}{2}\frac{\mu_\kappa}{\epsilon_\mu}\mathrm{Re}\left\{\Psi_1^\star(z)e^{i\alpha(C-z)^2/2}\int_1^z e^{-i\alpha(C-\zeta)^2/2}\left((C-\zeta)\frac{d\Psi_1}{d\zeta}(\zeta)+\Psi_1(\zeta)\right)d\zeta\right\}. \tag{59}$$

Note that F_α and G_α depend only on $\alpha = \alpha(L_{de}, V_r) = (\mu_m \Lambda)/(L_{de} V_r)$ and μ_κ. Significantly, the functions are independent of moisture parameters $\overline{Q}_r$ and G_s. We explore their interaction and effects on the meridional rainwater flux numerically.

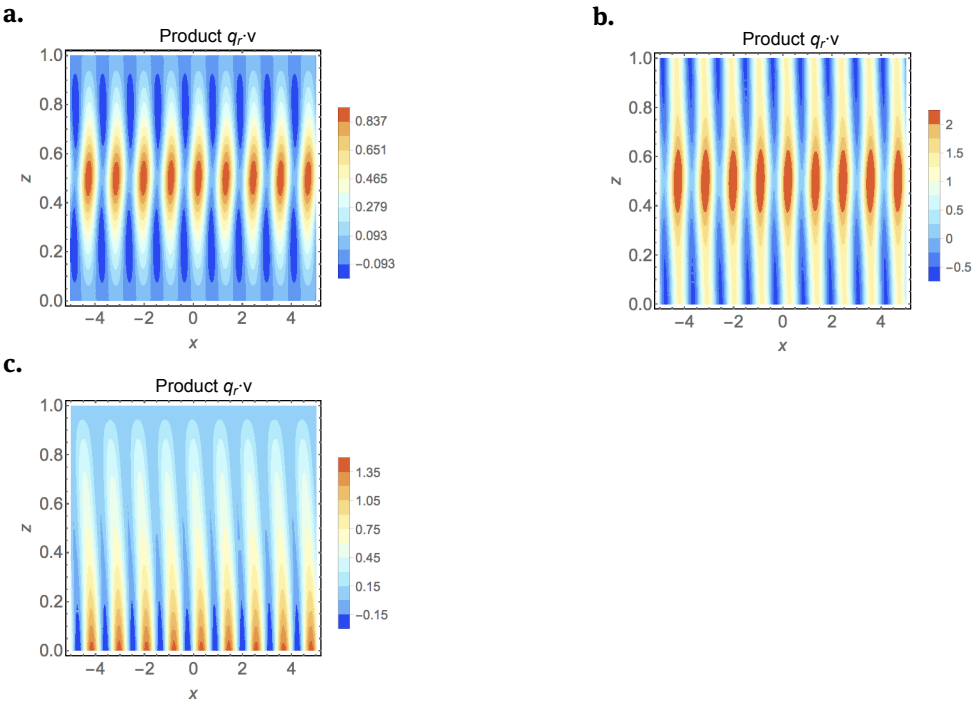

Figure 9: Product of rainwater vapor q_r with meridional velocity v: (panel **a.**) without background moisture gradient or rainfall precipitation $\overline{Q}_r = 0$, $V_r = 0$; (panel **b.**) without rainfall precipitation $\overline{Q}_r = 1$, $V_r = 0$; (panel **c.**) with rainfall precipitation $\overline{Q}_r = 1$, $V_r = 1$.

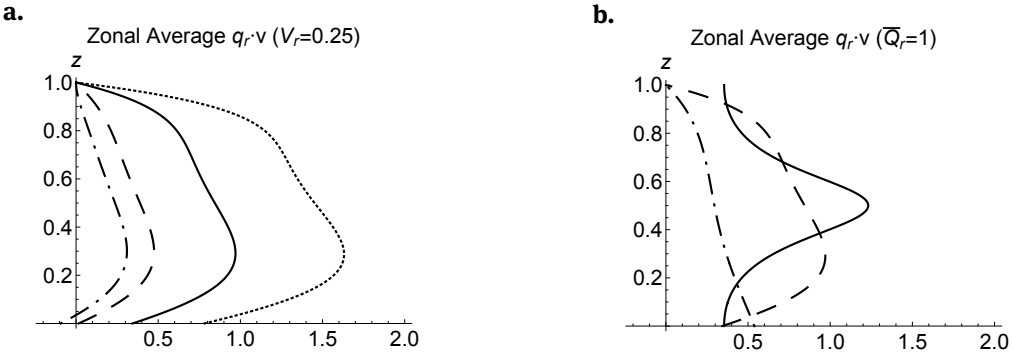

Figure 10: Zonal average of meridional rainwater flux $\langle v q_r \rangle$ (most unstable wavenumber only) as a function of height: (panel **a.**) different values of background moisture gradient with fixed precipitation speed (dash-dotted line $\overline{Q}_r = 0$, dashed line $\overline{Q}_r = 0.5$, solid line $\overline{Q}_r = 1$, dotted line $\overline{Q}_r = 2$) ; (panel **b.**) different values of precipitation speed with fixed background moisture gradient (solid line $V_r = 0$, dashed line $V_r = 0.25$, dash-dotted line $V_r = 1$).

We see from Figure 10 that the shape of the flux itself is heavily influenced by the rainfall speed V_r. Namely, the meridional flux $\langle v q_r \rangle$ achieves a global maximum at the center of the air column $z = 1/2$ for the value $V_r = 0$ (no sedimentation), regardless of the meridional gradient of moisture $\overline{Q}_r$. This maximum is reduced and moved downward by increasing values of V_r. For values $V_r \approx 0.65$ and above (with our nominal chosen

parameters), the global maximum of the flux ceases to occur in the interior of the air column; the global maximum is then found at the bottom boundary. We refer to the reader to Appendix C for a more detailed exploration.

Rainfall speed (sedimentation) is a significant contributor to the overall shape of the meridional moisture transport. A crude, yet useful, comparison of our meridional flux profiles with realistic zonally averaged meridional moisture transport profiles [25, Fig. 12.11b] suggests that non-zero rainfall speed is a necessary component for the verisimilitude of our model; compare solid curves of Figure 10 with Figure 12.11b of Peixoto and Oort [25] at 45° N,S. In particular, zonally averaged mid-latitude meridional moisture transport is observed to be poleward with a maximum near the surface in the northern hemisphere and a maximum above the surface (lower troposphere) in the southern hemisphere. This particular outcome is only captured in our fast microphysics, PQG model when $V_r > 0$. Therefore, it is not merely the existence of rainwater that is required, but sedimentation as a process itself is necessary for suitable comparisons with realistic water transport.

Lastly, we note that this simple model perhaps also captures one more important feature of northern and southern hemisphere meridional water fluxes. In the model, we find that the maximum of the zonally averaged water flux is moved downward toward the bottom surface in the case with rainfall ($V_r > 0$) as compared to the case without rainfall ($V_r = 0$). In observations, the zonally averaged water flux has a maximum that is closer to the surface in the northern hemisphere than in the southern hemisphere [25, Fig. 12.11b]. Together, these considerations suggest that the vertical location of this maximum may be related to the amount of precipitation. Indeed, it is the case that observed zonally averaged precipitation is slightly higher in Northern hemisphere than in the southern hemisphere at mid-latitudes; see, for example, Adler et al. [1, Fig. 5] and Béranger et al. [3, Fig. 4]. It would be interesting to make a more quantitative comparison in the future.

5 Conclusion

We have used a minimal thermodynamics and microphysics model in the QG limit (PQG model) to study the effects of moisture and rainfall speed on the mid-latitude meridional moisture transport. The PQG model arises from a systematic simplification of the anelastic equations of moist air with a suitable asymptotic expansion in the quasi-geostrophic limit [27]; no small-scale convection is present in the quasi-geostrophic limit, and no convective parametrization is used in the present study.

In this simplified setting, we studied the linear stability of the model under a constant velocity shear and use the accompanying normal mode solutions to construct zonally averaged water flux formulas. Essentially, the normal mode results correspond to a generalization of the Eady model of dry dynamics with modifications accounting for the inclusion of single-phase moisture, i.e., an uncoupled moisture equation plus an effective static stability parameter. In this QG limit, the stability of the solutions is only indirectly affected by the background moisture in the saturated regime. The stability of the unsaturated regime is unaffected by moisture. The meridional gradients of background water have the expected consequence of strengthening the meridional water anomaly flux, to compensate (or stabilize) this moisture imbalance. Rainfall speed (sedimentation) is found to have a significant impact on the structure of the rainwater and the location of greatest meridional flux. In this manner, rainfall speed breaks the vertical symmetry of the water flux, leading to more water accumulating at the bottom boundary.

Our results for different rainfall speed V_T values are consistent, at a crude level of comparison, with the different vertical profiles of observed zonally averaged moisture transport in the mid-latitude northern and southern hemispheres. Moreover, the fact that observed precipitation is larger in the northern versus southern hemisphere [1, 3], further lends credence to the rainwater transport results of this model; larger values of V_T lead to the mid-troposphere maximum of the zonally averaged rainwater flux moving downward. Since our solutions are linear, no direct quantitative comparison can be made. Nevertheless, this study suggests a potentially important role of rainfall in shaping the vertical structure of meridional moisture transport, and it would be interesting to investigate this potential connection in more detail in the future.

Acknowledgement: The authors gratefully acknowledge support from the U.S. National Science Foundation under grant NSF AGS–1443325 and thank Thomas K. Edwards and Jonathan E. Martin for many useful conversations and two anonymous reviewers for helpful comments.

Appendix

A Normalization of the Normal Modes

In this appendix we discuss the details of our normalization of the normal modes and other normalizations found in the literature. It is interesting to note that not all of these normalizations are equivalent in terms of the dependence on the moisture parameter L_D.

One possible normalization, and the one chosen in this paper, consists in normalizing the streamfunction by the initial energy $E(0) = E_0$. Namely, we choose c_1 in equation (31) so that $E_0 = 1$. Since the energy given by equations here is essentially dry energy, holding the energy constant makes for a sensible comparison between cases with differing levels of moisture.

Now, for periodic functions of the form (25),

$$\begin{aligned} E &= \frac{1}{2}\frac{k}{2\pi}\int_0^1\int_0^{2\pi/k}\left(u^2+v^2+b^2\right)\,dx\,dz \\ &= \frac{1}{4}\int_0^1 \mathrm{Re}\left\{U(z)U^\star(z)+V(z)V^\star(z)+B(z)B^\star(z)\right\}e^{2\,\mathrm{Im}\{\omega\}t}\,dz \\ &= c_1^2\frac{1}{4}\int_0^1 \mathrm{Re}\left\{(k^2+l^2)\Psi_1(z)\Psi_1^\star(z)+\frac{L^2}{L_D^2}\frac{d\Psi_1}{dz}(z)\frac{d\Psi_1}{dz}^\star(z)\right\}e^{2\,\mathrm{Im}\{\omega\}t}\,dz \\ &= c_1^2\frac{L^2}{L_D^2}e^{2\,\mathrm{Im}\{\omega\}t}\epsilon_\mu, \end{aligned} \tag{60}$$

where ϵ_μ is given in (37). We note that we do not take an integral in the y direction since for the most unstable mode $l = 0$ in the doubly periodic case and is taken to be $l \approx 0$ in the channel case. From equation (60) we conclude that normalizing so that the initial energy is equal to unity implies

$$c_1 = \frac{L_D}{L}\frac{1}{\sqrt{\epsilon_\mu}} \quad \text{or} \quad c_1 \propto \frac{L_D}{L}. \tag{61}$$

Similarly, we may have normalized the streamfunction by the kinetic energy as in Gall [11, pg. 1699]. This is essentially the same as assuming that the kinetic energy is chosen to be unity. This, in essence, gives the same scaling as that by the total energy and we find that the normalization scales the streamfunction as

$$c_1 \propto \frac{L_D}{L}. \tag{62}$$

A normalization in terms of (dry) energy is analogous to normalizing the streamfunction by, say, the maximum of the buoyancy. Namely, from equation (22) we see that to make the buoyancy independent of the deformation radius L_D, we require a scaling of the streamfunction of the form (62). This type of normalization is perhaps the most physically sensible since the buoyancy in the quasi-geostrophic limit corresponds to the potential temperature θ; a quantity that should not be affected by the addition of moisture.

Another form of normalization is that chosen in Bannon [2] or Mak [19], in which one sets the top layer zonal velocity equal to unity. In the context of our system of equations this requires for a scaling of the form

$$c_1 \propto \frac{1}{k} \propto \frac{L_D}{L}. \tag{63}$$

The fact that c_1 would be proportional to L_D/L holds true for the most unstable wavenumber ($l \approx 0$).

Lastly, if instead we chose to normalize as in Fantini [9, pg. 1284] with the maximum of vertical velocity equal to unity, we find from (27b) that

$$c_1 \propto \frac{1}{k}\left(\frac{L_D}{L}\right)^2 \propto \left(\frac{L_D}{L}\right)^3. \tag{64}$$

B Zonal Mean

For any functions

$$a(x,y,z,t) = \mathrm{Re}\left\{A(z)e^{i(kx+ly-\omega t)}\right\} = |A(z)|\cos(kx+ly-\mathrm{Re}\{\omega\}t+\phi_A(z))e^{\mathrm{Im}\{\omega\}t} \tag{65}$$

and

$$b(x,y,z,t) = \mathrm{Re}\left\{B(z)e^{i(kx+ly-\omega t)}\right\} = |B(z)|\cos(kx+ly-\mathrm{Re}\{\omega\}t+\phi_B(z))e^{\mathrm{Im}\{\omega\}t} \tag{66}$$

with the structure of the doubly periodic normal mode solutions, taking the zonal mean gives the following simplified result:

$$\begin{aligned}\frac{k}{2\pi}\int_0^{2\pi/k} a(x,y,z,t)b(x,y,z,t)\,dx &= \frac{k}{2\pi}\int_0^{2\pi/k} |A(z)|\cos\left(kx+ly-\mathrm{Re}\{\omega\}t+\phi_A(z)\right)\\ &\qquad |B(z)|\cos(kx+ly-\mathrm{Re}\{\omega\}t+\phi_B(z))\,dx\,e^{2\,\mathrm{Im}\{\omega\}t}\\ &= \frac{1}{2}|A(z)||B(z)|\cos\left(\phi_A(z)-\phi_B(z)\right)e^{2\,\mathrm{Im}\{\omega\}t}\\ &= \frac{1}{2}\mathrm{Re}\left\{A(z)B^\star(z)\right\}e^{2\,\mathrm{Im}\{\omega\}t}.\end{aligned} \tag{67}$$

Note that this does not mean that the wavenumber l has no consequence on the zonal average (or flux) in question. The coefficients $A(z)$, $B(z)$ may depend on the wavenumber l even if explicit y dependence does not appear in the final result.

Similarly, if the functions a, b had the structure of channel normal mode solutions we have

$$\frac{k}{2\pi}\int_0^{2\pi/k} a(x,y,z,t)b(x,y,z,t)\,dx = \frac{1}{2}\mathrm{Re}\left\{A(z)B^\star(z)\right\}\cos^2(ly)e^{2\,\mathrm{Im}\{\omega\}t} \tag{68}$$

generically for the zonal mean. Unlike the doubly periodic solutions, note that this expression contains explicit dependence on the wavenumber l.

C Dependence of Zonally Averaged Meridional Rainwater Flux on Moisture Parameters

In this appendix, we discuss, in slightly more detail, the dependence of the zonal average of meridional rainwater flux $\langle vq_r\rangle$ on the moist parameters $\overline{Q}_r$ and V_r; see Figure 11. First, a strong meridional rainwater gradient $L_{de}\overline{Q}_r/(L\Lambda) \gg G_s$ forces the meridional rainwater flux $\langle vq_r\rangle$ to be positive (northward) throughout the air column, while a weak gradient $L_{de}\overline{Q}_r/(L\Lambda) \ll G_s$ allows the rainwater flux to become negative (southward) near the bottom surface of the domain for certain values of V_r. Second, even if the meridional background gradient is strong enough to make $\langle vq_r\rangle$ strictly positive, a local minimum of the flux is located above the bottom boundary. This minimum appears for $Vr \approx 0.095$ and merges into the bottom boundary for $Vr \approx 0.16$ when using our nominal parameter values ($\overline{Q}_r = 1$); a weaker value of $\overline{Q}_r$ will allow this minimum to develop for smaller values of V_r and persist to higher values of V_r. This is in contrast to the unsaturated and saturated $V_r = 0$ cases, in which the meridional flux is strictly positive (northward) and no local minimum may form above the bottom surface. Third, the large peak visible in Figure 11 at the top of the domain for small V_r arises due to our chosen boundary condition and is presumably not physical. Namely, the fact that $V_r \to 0$ is a singular limit of the rainwater equation leads to this boundary layer effect.

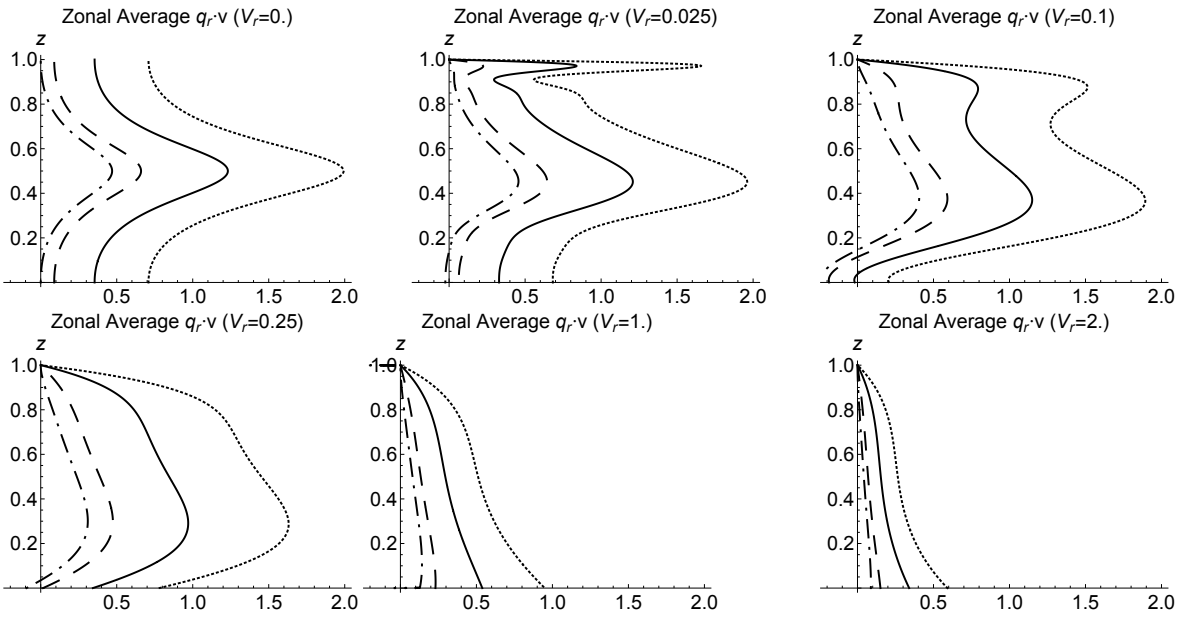

Figure 11: Zonal average of meridional rainwater flux $\langle vq_r \rangle$ (most unstable wavenumber only) as a function of height for different values of precipitation speed. In each plot four curves are plotted: flux with no meridional rainwater gradient ($\overline{Q}_r = 0$; dash-dotted line), weak meridional gradient ($\overline{Q}_r = 0.5$; dashed line), moderate meridional gradient ($\overline{Q}_r = 1$; solid line), and strong meridional gradient ($\overline{Q}_r = 2$; dotted line).

References

[1] Robert F. Adler, George J. Huffman, Alfred Chang, Ralph Ferraro, Ping-Ping Xie, John Janowiak, Bruno Rudolf, Udo Schneider, Scott Curtis, David Bolvin, Arnold Gruber, Joel Susskind, Philip Arkin, and Eric Nelkin. The version-2 global precipitation climatology project (GPCP) monthly precipitation analysis (1979–present). *J. Hydrometeor.*, 4(6):1147–1167, 2003. 10.1175/1525-7541(2003)004<1147:TVGPCP>2.0.CO;2.

[2] Peter R. Bannon. Linear development of quasi-geostrophic baroclinic disturbances with condensational heating. *J. Atmos. Sci.*, 43(20):2261–2274, 1986. 10.1175/1520-0469(1986)043<2261:LDOQGB>2.0.CO;2.

[3] Karine Béranger, Bernard Barnier, Sergei Gulev, and Michel Crépon. Comparing 20 years of precipitation estimates from different sources over the world ocean. *Ocean Dyn.*, 56(2):104–138, 2006. 10.1007/s10236-006-0065-2.

[4] J. G. Charney. The dynamics of long waves in a baroclinic westerly current. *J. Meteor.*, 4(5):135–162, 1947. 10.1175/1520-0469(1947)004<0136:TDOLWI>2.0.CO;2.

[5] Hylke de Vries, John Methven, Thomas H. A. Frame, and Brian J. Hoskins. Baroclinic waves with parameterized effects of moisture interpreted using rossby wave components. *J. Atmos. Sci.*, 67(9):2766–2784, 2010. 10.1175/2010JAS3410.1.

[6] Dale R. Durran and Joseph B. Klemp. On the effects of moisture on the Brunt-Väisälä frequency. *J. Atmos. Sci.*, 39(10): 2152–2158, 1982. 10.1175/1520-0469(1982)039<2152:OTEOMO>2.0.CO;2.

[7] E. T. Eady. Long waves and cyclone waves. *Tellus A*, 1(3):33–52, 1949. 10.1111/j.2153-3490.1949.tb01265.x.

[8] Kerry A. Emanuel, Maurizio Fantini, and Alan J. Thorpe. Baroclinic instability in an environment of small stability to slantwise moist convection. Part I: Two-dimensional models. *J. Atmos. Sci.*, 44(12):1559–1573, 1987. 10.1175/1520-0469(1987)044<1559:BIIAEO>2.0.CO;2.

[9] Maurizio Fantini. Nongeostrophic corrections to the eigensolutions of a moist baroclinic instability problem. *J. Atmos. Sci.*, 47(11):1277–1287, 1990. 10.1175/1520-0469(1990)047<1277:NCTTEO>2.0.CO;2.

[10] Dargan M. W. Frierson, Isaac M. Held, and Pablo Zurita-Gotor. A gray-radiation aquaplanet moist GCM. Part I: Static stability and eddy scale. *J. Atmos. Sci.*, 63(10):2548–2566, 2006. 10.1175/JAS3753.1.

[11] Robert Gall. The effects of released latent heat in growing baroclinic waves. *J. Atmos. Sci.*, 33(9):1686–1701, 1976. 10.1175/1520-0469(1976)033<1686:TEORLH>2.0.CO;2.

[12] Balasubramanian Govindasamy and S. T. Garner. The equilibration of short baroclinic waves. *J. Atmos. Sci.*, 54(24):2850–2871, 1997. 10.1175/1520-0469(1997)054<2850:TEOSBW>2.0.CO;2.

[13] Gerardo Hernández-Dueñas, Andrew J. Majda, Leslie M. Smith, and Samuel N. Stechmann. Minimal models for precipitating turbulent convection. *J. Fluid Mech.*, 717:576–611, 2 2013. 10.1017/jfm.2012.597.

[14] Gerardo Hernández-Dueñas, Leslie M. Smith, and Samuel N. Stechmann. Stability and instability criteria for idealized precipitating hydrodynamics. *J. Atmos. Sci.*, 72(6):2379–2393, 2015. 10.1175/JAS-D-14-0317.1.

[15] James R. Holton and Gregory J. Hakim. *An Introduction to Dynamic Meteorology*. Academic Press, Boston, MA, 2013.

[16] Frédéric Laliberté, Tiffany Shaw, and Olivier Pauluis. Moist recirculation and water vapor transport on dry isentropes. *J. Atmos. Sci.*, 69(3):875–890, 2012. 10.1175/JAS-D-11-0124.1.

[17] Julien Lambaerts, Guillaume Lapeyre, and Vladimir Zeitlin. Moist versus dry baroclinic instability in a simplified two-layer atmospheric model with condensation and latent heat release. *J. Atmos. Sci.*, 69(4):1405–1426, 2012. 10.1175/JAS-D-11-0205.1.

[18] G. Lapeyre and I. M. Held. The role of moisture in the dynamics and energetics of turbulent baroclinic eddies. *J. Atmos. Sci.*, 61(14):1693–1710, 2004. 10.1175/1520-0469(2004)061<1693:TROMIT>2.0.CO;2.

[19] Mankin Mak. On moist quasi-geostrophic baroclinic instability. *J. Atmos. Sci.*, 39(9):2028–2037, 1982. 10.1175/1520-0469(1982)039<2028:OMQGBI>2.0.CO;2.

[20] John Marshall and R. Alan Plumb. *Atmosphere, Ocean, and Climate Dynamics: An Introductory Text*. Academic Press, Boston, MA, 2007.

[21] Joy M. Monteiro and Jai Sukhatme. Quasi-geostrophic dynamics in the presence of moisture gradients. *Quart. J. Roy. Meteor. Soc.*, 142(694):187–195, 2016. 10.1002/qj.2644.

[22] Paul A. O'Gorman. The effective static stability experienced by eddies in a moist atmosphere. *J. Atmos. Sci.*, 68(1):75–90, 2011. 10.1175/2010JAS3537.1.

[23] Olivier Pauluis, Arnaud Czaja, and Robert Korty. The global atmospheric circulation on moist isentropes. *Science*, 321(5892): 1075–1078, 2008. 10.1126/science.1159649.

[24] Joseph Pedlosky. *Geophysical Fluid Dynamics*. Springer-Verlag, New York, NY, 1987.

[25] J. P. Peixoto and A. H. Oort. *Physics of Climate*. American Institute of Physics, New York, NY, 1992.

[26] R. Richiardone and F. Giusti. On the stability criterion in a saturated atmosphere. *J. Atmos. Sci.*, 58(14):2013–2017, 2001. 10.1175/1520-0469(2001)058<2013:OTSCIA>2.0.CO;2.

[27] Leslie M. Smith and Samuel N. Stechmann. Precipitating quasi-geostrophic equations and potential vorticity inversion with phase changes. 2017. submitted.

[28] Kevin E. Trenberth and Julie M. Caron. Estimates of meridional atmosphere and ocean heat transports. *J. Climate*, 14(16): 3433–3443, 2001. 10.1175/1520-0442(2001)014<3433:EOMAAO>2.0.CO;2.

[29] Kevin E. Trenberth and David P. Stepaniak. Covariability of components of poleward atmospheric energy transports on seasonal and interannual timescales. *J. Climate*, 16(22):3691–3705, 2003. 10.1175/1520-0442(2003)016<3691:COCOPA>2.0.CO;2.

[30] G. K. Vallis. *Atmospheric and Oceanic Fluid Dynamics*. Cambridge University Press, Cambridge, U.K., 2006.

[31] Bin Wang and Albert Barcilon. Moist stability of a baroclinic zonal flow with conditionally unstable stratification. *J. Atmos. Sci.*, 43(7):705–719, 1986. 10.1175/1520-0469(1986)043<0705:MSOABZ>2.0.CO;2.